Research Square

Preprints are preliminary reports that have not undergone peer review.
They should not be considered conclusive, used to inform clinical practice,
or referenced by the media as validated information.

Mach reflections of a cellular detonation over a convex–concave cylindrical surface

Chenyu Yao
Hefei University of Technology
Xiao Ma
China Academy of Engineering Physics
Quan Li
quanli@hfut.edu.cn

Hefei University of Technology

Research Article

Keywords: Mach reflection, Convex-concave surface, Cellular detonation, Critical wedge angle

Posted Date: November 19th, 2026

DOI: https://doi.org/10.21203/rs.3.rs-11570875/v1

License: This work is licensed under a Creative Commons Attribution 4.0 International License.
Read Full License

Additional Declarations: No competing interests reported.

Mach reflections of a cellular detonation over a convex–concave cylindrical surface

Chenyu Yao[1], Xiao Ma[2], Quan Li[1*]*

[1]School of Civil Engineering, Hefei University of Technology, Hefei, Anhui 230009, China

[2]National Key Laboratory of Shock Wave and Detonation Physics, Institute of Fluid Physics, China Academy of Engineering Physics, 621900 Mianyang, China

Abstract

Mach reflections of a cellular detonation over convex–concave coupled wedges were experimentally and numerically studied, using a combination of high-speed schlieren imaging and soot foil technology. The 4.41-m long, 8.0-cm square cross-section modular channel was equipped with a convex-concave cylindrical surface or a single concave wedge (as a benchmark case) in the optical section. Stoichiometric hydrogen-oxygen mixtures diluted with different argon amounts were tested at an initial pressure of 10–40 kPa. The results indicate that the coupled wedge induces two Mach reflections: one occurs when the incident detonation wave reflects off the forward convex surface, and the other occurs when the first Mach stem reflects off the rear concave surface. The second Mach reflection on the rear concave surface is observed to be delayed relative to that on a single concave wedge owing to the influence of the forward wedge. For the convex–concave wedges, the geometric size of the forward wedge is found not to affect the first Mach reflection, but to affect the second Mach reflection on the rear concave surface.

Keywords: Mach reflection, Convex-concave surface, Cellular detonation, Critical wedge angle

1 Introduction

Understanding the complex flows associated with detonation reflection off different geometries is important for applications such as detonation-based propulsion and explosion protection, where substantial changes in pressure and temperature can occur. Early investigations of shock reflection date back to the work of Mach [1], who studied the problem of inert shock reflection. The shock reflection phenomenon occurs either when a shock wave impinges on a planar surface inclined at an angle, or when a supersonic flow propagates towards a planar surface. There are two possible reflection configurations, regular reflection (RR) and Mach reflection (MR), governed by the shock Mach numbers, incidence angle and geometry. RR is characterized by an incident shock wave and a reflected wave that meet at a single point on the reflecting surface. MR has an additional shock wave, Mach stem, that is perpendicular to the reflecting surface. The difference in post-wave thermodynamic states between the Mach stem and the reflected wave leads to the formation of a slipstream. The three waves and the slipstream meet at a single point, known as the triple point, which travels along a trajectory at an angle to the reflecting surface.

The criterion for the transitions from RR to MR in pseudo-steady and steady flow reflections was well established by Ben-Dor [2]. The RR configuration can be solved by two-shock theory developed by von Neumann [3]; the MR configuration can be described by three-shock theory [4], as well as the Chester-Chisnell-Whitham (CCW) theory [5–7]. Unsteady shock wave reflection is substantially more complex relative to pseudo-steady and steady reflection. Generally, the unsteady reflections form as the reflecting surface angle changes continuously and the reflection is continually adapting to the boundary conditions. On a concave surface, the

incident shock develops into a direct Mach reflection (DiMR); as the shock advances, this transitions to an inverse Mach reflection (InMR) with the triple point (TP) moving towards the surface. The InMR eventually transforms into a transitioned regular reflection (TRR) upon the collision of the TP with the surface. Similar to pseudo-steady and steady reflections, the reflection begins as an RR and then transitions into an MR on a convex surface. The main difference is that the RR→MR transition occurs at smaller angles than those predicted by the established theories in both pseudo-steady and steady flows. Further investigations of reflections over coupled surfaces were conducted to study unsteady RR→MR and MR→RR transitions. Skews and Blitterswijk [8] studied unsteady reflection off a leading circular section joined to a plane wall section. They suggested that the reflected wave profile requires a finite time to adapt to the new boundary conditions due to the continuously changing reflecting surface. Geva et al. [9] studied the unsteady MR→RR and RR→MR transitions on a cylindrical concave-convex surface and found that the hysteresis phenomenon occurred in a transient flow at a lower incident shock Mach number than in steady flows.

Unlike an inert shock wave, a detonation wave has a finite thickness; thus, the characteristic length scale breaks the self-similarity of the MR process. Furthermore, the known theories based on the assumption of self-similarity in pseudo-steady and steady flows are not applicable for analyzing the non-self-similar MR process. In studies of shock reflection with relaxation, Hornung et al. [10–11] established the frozen and equilibrium limits for the MR process in the near and far fields, respectively. These classifications were later applied to detonations by Shepherd et al. [12]. Further experimental and numerical work [13–15] has corroborated the existence of these two limits for Mach reflection in detonations. Recently, the pursuit of detonation-based engines has stimulated considerable interest in understanding detonation reflections on complex boundaries. Yuan et al. [16] conducted numerical simulations of detonation reflection off a concave surface. They found that the detonation undergoes DiMR, InMR, and TRR, a transition sequence identical to that of an inert shock. Jiao et al. [17] experimentally confirmed the reflection-type transition of a detonation on a concave surface. Their results showed that Mach reflection terminates earlier than predicted by the reactive CCW theory. As for reflection on convex surfaces, the RR→MR process cannot be analyzed by the established theories, because the convex geometries exert an expansive influence on the detonation [18]. Li et al. [19] confirmed that the MR process does not follow the frozen limit when a strong expansion is introduced.

Reflection structures of detonations on both single convex and single concave surfaces have been comprehensively studied. The present study aims to advance the understanding of detonation reflection dynamics, focusing on the unsteady case of a Chapman-Jouguet (CJ) detonation wave propagating over a coupled convex-concave wedge. It is believed that the detonation wave reflection structures formed on the first reflector would endure on the second. Thus, the findings indicate that the reflection process over the second reflector differs completely from that over a single-concave reflector; this is because the Mach stem generated on the leading convex surface acts as the incident wave over the second reflector. In particular, the last transition (InMR→TRR) occurs later than one would expect when the detonation reflects off a single-concave surface. To clarify the underlying reflection dynamics, a series of numerical simulations were performed with various reflector geometries. From a practical standpoint, the study of detonation reflection on coupled reflecting surfaces is critically

important, as it is closely related to applications in aeronautical and military industries, such as pulsed and rotating detonation engines.

2 Experiments

The experiments were conducted in a 4.41-m-long aluminum modular channel with an 80-mm square cross-section. The channel comprises four sections: a detonation initiation section, a propagation section, a test section and a dump tank (Fig. 1a). Modules 2–4 were fitted with semi-cylindrical obstacles on the top and bottom walls to promote detonation formation, whereas the propagation section had smooth walls to ensure a planar CJ detonation wave. The test section was equipped with 30-mm-thick quartz glass windows to provide a field-of-view of 466 × 80 mm and was internally lined with 2-mm-thick sacrificial quartz glass. The windows provided optical access for schlieren photography at up to 160,000 frames per second (fps) with a Photron SA-Z high-speed camera. The resolution of the high-speed camera was 512 × 128 pixels with an exposure time of 159 ns. The single-pass schlieren setup consisted of a 100 W xenon arc lamp light source, and two 300-mm-diameter concave mirrors. In addition to the schlieren visualization, a soot foil technique was employed to record the cellular structure and triple-point trajectory of Mach reflection. This was accomplished by uniformly sooting an aluminum sheet with dimensions of 438 × 118 × 0.5 mm and placing it on the inside of the quartz glass window. Four different curved-surface wedges shown in Fig. 1b, which provided the surface for Mach reflection, were installed in the test section. Dimensions of the wedges are listed in Table 1. W#1 was a single concave surface with a radius (R_2) of 30 mm, serving as a benchmark case. The convex-concave coupled wedges (W#2, #3 and #4) have an identical concave surface (R_2 = 30 mm) but different convex radii (R_1 = 20 mm, 30 mm and 40 mm).

The mixtures were stoichiometric hydrogen–oxygen mixtures with different levels of argon dilution, i.e., $2H_2$–O_2–2Ar and $2H_2$–O_2–4.5Ar. Each of them was prepared in a separate mixing chamber using the partial-pressure method and was allowed to mix for more than 24 h. Prior to filling with the test mixture before each experiment, the channel was evacuated to an absolute pressure below 100 Pa. All tests were performed at a temperature of 298 K and an initial pressure in the range of 10–40 kPa. The mixture was ignited from the left end of the channel by an automotive spark plug supplemented with a capacitive discharge system, delivering a spark energy of 500 mJ.

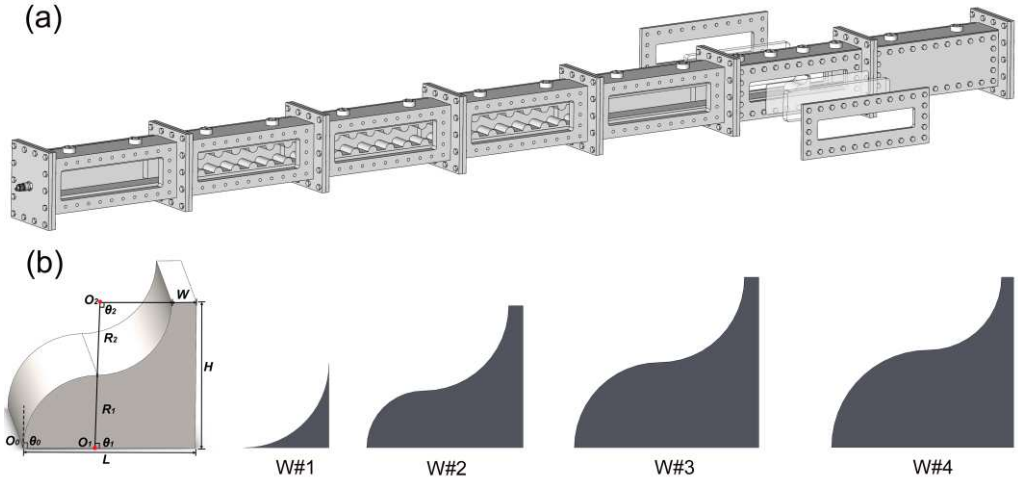


Fig. 1. Experimental setup, (a) combustion channel, (b) convex-concave coupled wedges.

Table 1. Parameter of convex-concave coupled wedges

No.	θ_1 (°)	R_1 (mm)	θ_2 (°)	R_2 (mm)	θ_0 (°)	W (mm)	L (mm)	H (mm)
W#1				30	90		30	30
W#2	90	20	90	30	90	10	80	70
W#3	90	30	90	30	90	10	60	50
W#4	90	40	90	30	90	10	70	60

3 Results and discussion

3.1 Mach reflection on a cylindrical concave surface

As a benchmark, Fig. 2 shows soot-foil records of a cellular detonation wave reflecting off a concave cylindrical surface with a radius of 30 mm (W#1) in a stoichiometric $2H_2$–O_2–2Ar mixture at different initial pressures (P_i). Unlike reflection from a planar wedge [15], a concave surface provides a continuously changing angle of incidence to the incident wave, resulting in more complex reflection dynamics. Specifically, upon interacting with the concave surface, the wave reflection evolves sequentially through direct Mach reflection (DiMR), stationary Mach reflection (StMR), inverse Mach reflection (InMR), and finally transitional regular reflection (TRR). Similar to normal Mach reflection, the triple-point trajectory (TPT), i.e., the dashed lines in Fig. 2, divides the cellular pattern into two distinct regions. The region above the TPT is characterized by very regular cells (the scaled cell width λ/λ_{CJ} = 0.96 to 1.02), typically indicative of CJ detonation waves; below the TPT, in the Mach stem region, the cellular structure becomes increasingly distorted and refined as a result of the overdriven state.

To study the reflections quantitatively, the Mach stem height H_m, obtained by extracting the coordinates of points on this trajectory at fixed distance intervals, is plotted as a function of θ in Fig. 3. Also shown are the predictions based on inert and reactive CCW theory [5–7]. Upon reflection off the concave surface, DiMR is immediately generated at which it produced a small tangential wedge angle θ. Because the flow behind the triple point has a positive angle with the surface where the Mach stem stands in the process of DiMR, the fluid correspondingly deviates from the wedge surface, driving the growth of the Mach stem ($\frac{\mathrm{d}Hm}{\mathrm{d}\theta} > 0$). Later, the increase of θ turns the flow to deviate towards the wedge surface, the Mach stem does not grow further as the flow is parallel to the wedge surface ($\frac{\mathrm{d}Hm}{\mathrm{d}\theta} = 0$), corresponding to the StMR configuration. Of note, StMR is transient because of the constant increase of θ with the detonation wave propagation, which ends at achieving a largest H_m. The angle between the flow and the wedge surface becomes negative as θ further increases, therefore Mach stem is shortened ($\frac{\mathrm{d}Hm}{\mathrm{d}\theta} < 0$), forming the structure of InMR. The InMR vanishes as the Mach reflection transitions to the TRR ($H_m = 0$). It is observed that P_i does not alter the reflection sequences of the incident wave, but instead affects the trend of H_m, e.g., H_m asymptotes to the reactive CCW line as P_i increases, especially for the InMR.

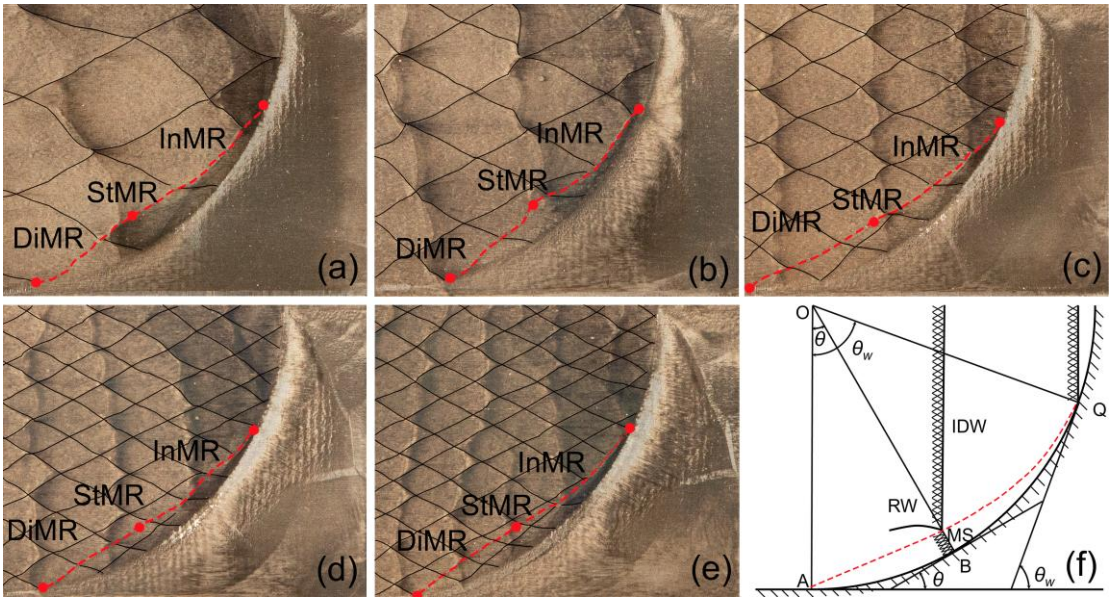


Fig. 2. Soot-foil records showing the reflection sequences of a cellular detonation wave over the concave wedge (W#1) in a stoichiometric $2H_2$–O_2–2Ar mixture, (a) P_i = 15 kPa, (b) P_i = 20 kPa, (c) P_i = 25 kPa, (d) P_i = 30 kPa, (e) P_i = 35 kPa, (f) schematic. DiMR-direct Mach reflection, StMR-stationary Mach reflection, InMR-inverse Mach reflection, TRR-transitioned regular reflection, RW-reflected wave, IDW-incident detonation wave, MS-Mach stem.

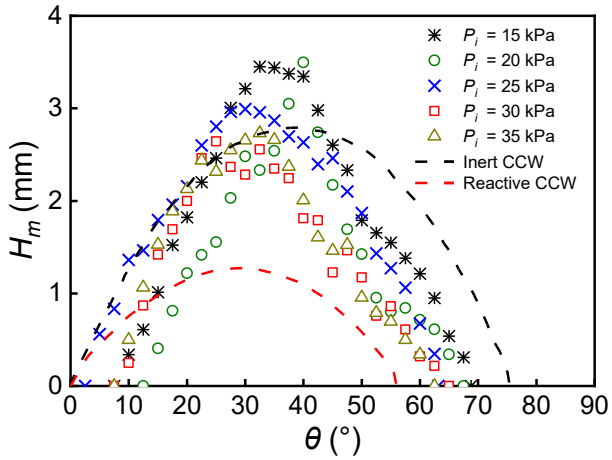


Fig. 3. Mach stem height H_m as a function of tangential wedge angle θ at different initial pressures.

3.2 Mach reflections on a convex-concave cylindrical surface

Compared to the benchmark in *Section 3.1*, the reflection of a cellular detonation wave becomes more complex when a convex surface is smoothly connected to the concave wedge. Fig. 4 shows the sequence of the schlieren images of Mach reflections on the convex-concave wedge (W#3) in $2H_2$–O_2–2Ar mixture at different initial pressures. The detonation wave typically undergoes a transition from regular reflection to Mach reflection on the front convex surface when the tangential angle α decreases from 90° to a critical value (see frames 1 and 2). The classical triple-waves structure is observed in frame 2, where the triple point links incident detonation wave, transverse wave (reflected wave) and Mach stem. Note that Mach stem is roughly perpendicular to the surface at the beginning. Subjected to the curvature, the foot of Mach stem maintains locally perpendicular to the surface, while the upper portion retains its

original angle, resulting in an arched Mach stem (highlighted by dashed lines in frame 3). Also in frame 3, the Mach stem approaches the junction of the convex and concave surfaces, indicating that the following reflection is governed by the concave configuration. Subsequent to frame 3, the Mach stem plays a role of incident wave, however it is not planar as the incident wave in benchmark in *Section 3.1*. Similarly, the Mach stem induces a new Mach reflection on the concave surface as α increases from 0 to a critical wedge angle in frame 4. For the sake of clarity, the Mach stem on the convex surface is denoted as MS_1 and that on the concave surface is designated as MS_2. After the second Mach reflection, the wave front now comprises the incident detonation wave, MS_1 and MS_2. Upon exceeding the critical angle, α triggers a transition from Mach reflection to regular reflection (see frame 5). Subsequently, as the incident detonation wave approaches the opening, MS_1 is completely engulfed by the concave surface. This occurs because the growth in the height of MS_1 is slower than the increase in the wall height of the concave wedge.

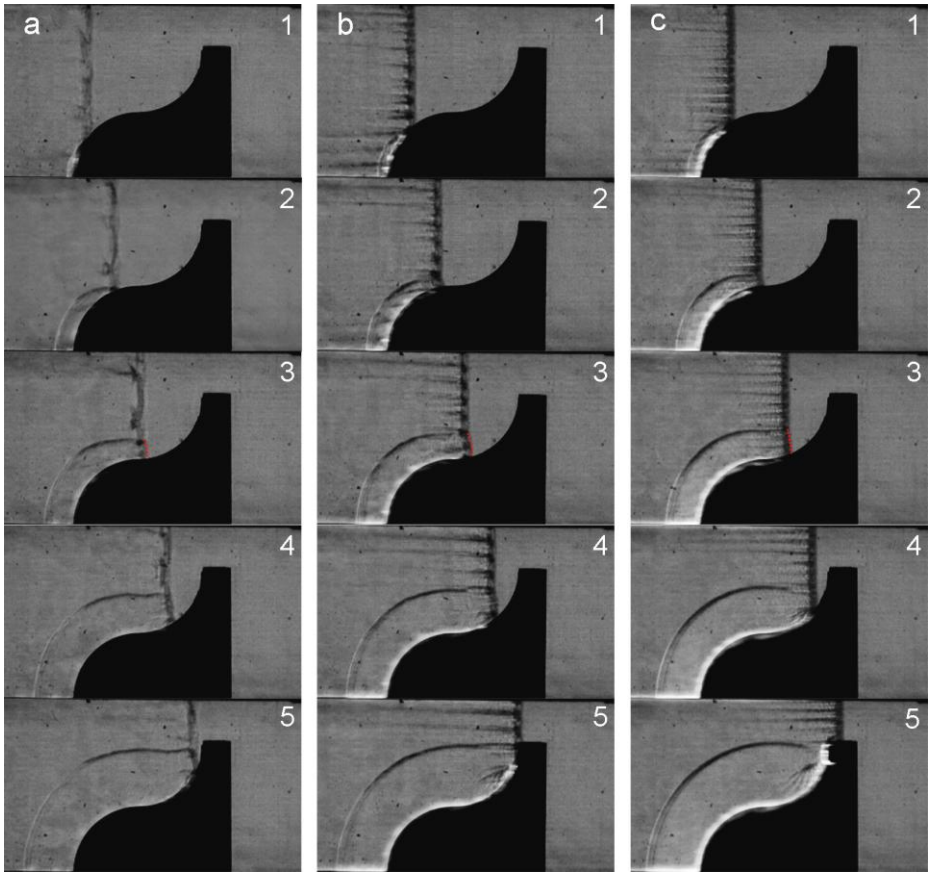


Fig. 4. Schlieren images showing the reflection sequences of a cellular detonation wave over a coupled convex-concave wedge (W#3) in a stoichiometric $2H_2$–O_2–2Ar mixture, (a) P_i = 10 kPa, (b) P_i = 20 kPa, (c) P_i = 30 kPa.

Since Mach reflection on the concave surface occurs on both a very small spatial scale and an even shorter temporal scale, its details are difficult to resolve using schlieren photography solely. To deepen the understanding of Mach reflections on these wedges, we employed soot foils to record the cellular pattern, as shown in Fig. 5. Two triple-point trajectories highlighted by the dashed lines are derived by analyzing differences in the cell size and features, which partition the cellular pattern into three distinct regions. Region 1 is the undisturbed CJ detonation region, where the cellular structure is relatively regular; region 2 is swept by MS_1,

and the cellular shape is deformed due to the overdriven Mach stem; region 3 is swept by MS_2, and the cellular pattern becomes more distorted and fine. It is observed that the first triple-point trajectory (TPT_1) originates approximately from the midpoint of the convex surface and terminates near the upper corner of the concave surface. The critical wedge angle θ'_{TPT1} corresponding to Mach reflection over the convex surface is 45.7°, 44.0°, 40.2° and 44.9° for 15 kPa, 20 kPa, 25 kPa and 30 kPa, respectively. The data indicated that the onset position of Mach reflection over the convex surface is independent of the initial pressure. However, it does affect the endpoint of TPT_1 by altering the height of MS_1, as evidenced by the decrease in the included angle θ''_{TPT1} measured at the termination of TPT_1 with increasing initial pressure, i.e., θ''_{TPT1} = 86°, 85.5°, 84.3° and 81.6° for 15 kPa, 20 kPa, 25 kPa and 30 kPa, respectively. A second triple-point trajectory (TPT_2) lies below TPT_1, associated with the Mach reflection of MS_1 off the concave surface. Similar to the benchmark in *Section 3.1*, TPT_2 also includes DiMR, StMR, InMR and TRR. It is noteworthy that prior to their final collisions with the wall surface, TPT_1 and TPT_2 remain non-intersecting throughout, indicating that no corner signal is transmitted between them.

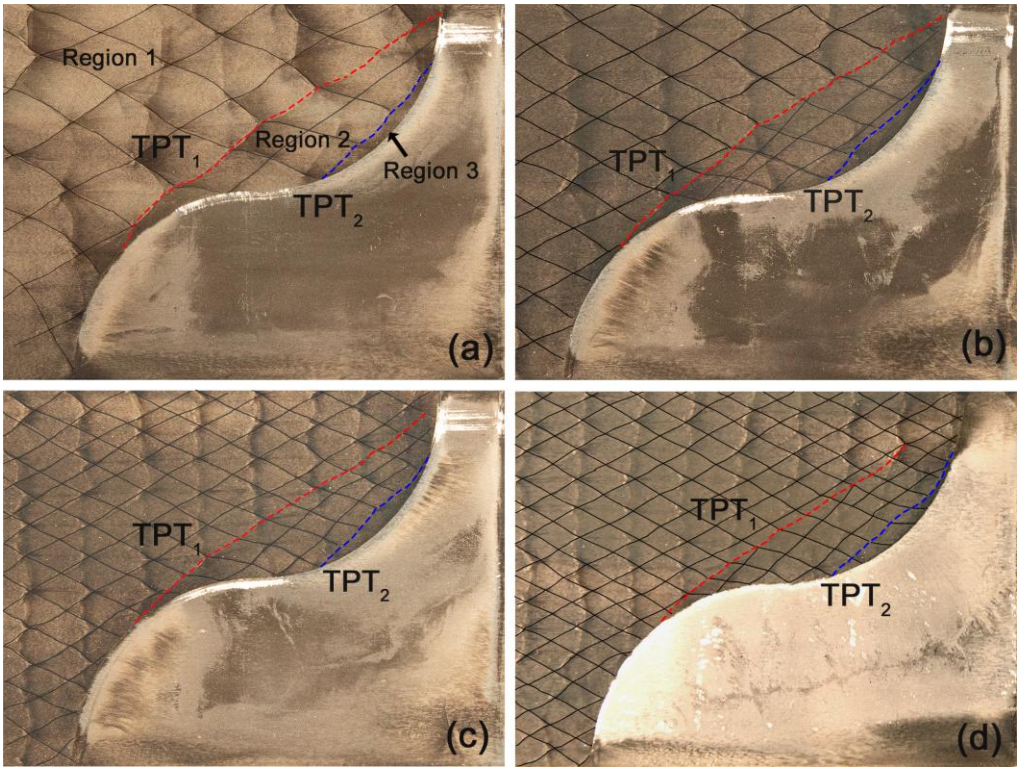


Fig. 5. Soot foil records showing the reflection sequences of a cellular detonation wave over W#3 in a stoichiometric $2H_2$–O_2–2Ar mixture, (a) P_i = 15 kPa, (b) P_i = 20 kPa, (c) P_i = 25 kPa, (d) P_i = 30 kPa.

The normalized MS_2 height H_m/R over the concave surface of W#3 is compared to that of MS_1 over W#1 in Fig. 6. Also shown for reference are the calculated H_m/R by the inert and reactive CCW theory. H_m/R shows a similar trend for W#1 and W#3 that increases to a maximum and then decreases to zero, corresponding to the sequences from DiMR, StMR, InMR to TRR for TPT_2. The significant difference is that the rightward shift of H_m/R for W#3 compared to that for W#1, indicating that Mach reflection over the concave surface of W#3 consistently occurs later than that over W#1. Recall that the Mach stem generated at the front convex surface of W#3 acted as an incident wave for Mach reflection over the concave surface,

and this incident wave has a larger incident angle compared to that formed by a CJ detonation wave over W#1. Mach reflection over the concave surface of W#3 does not occur from the Mach stem immediately until the incident angle decreases to a critical value.

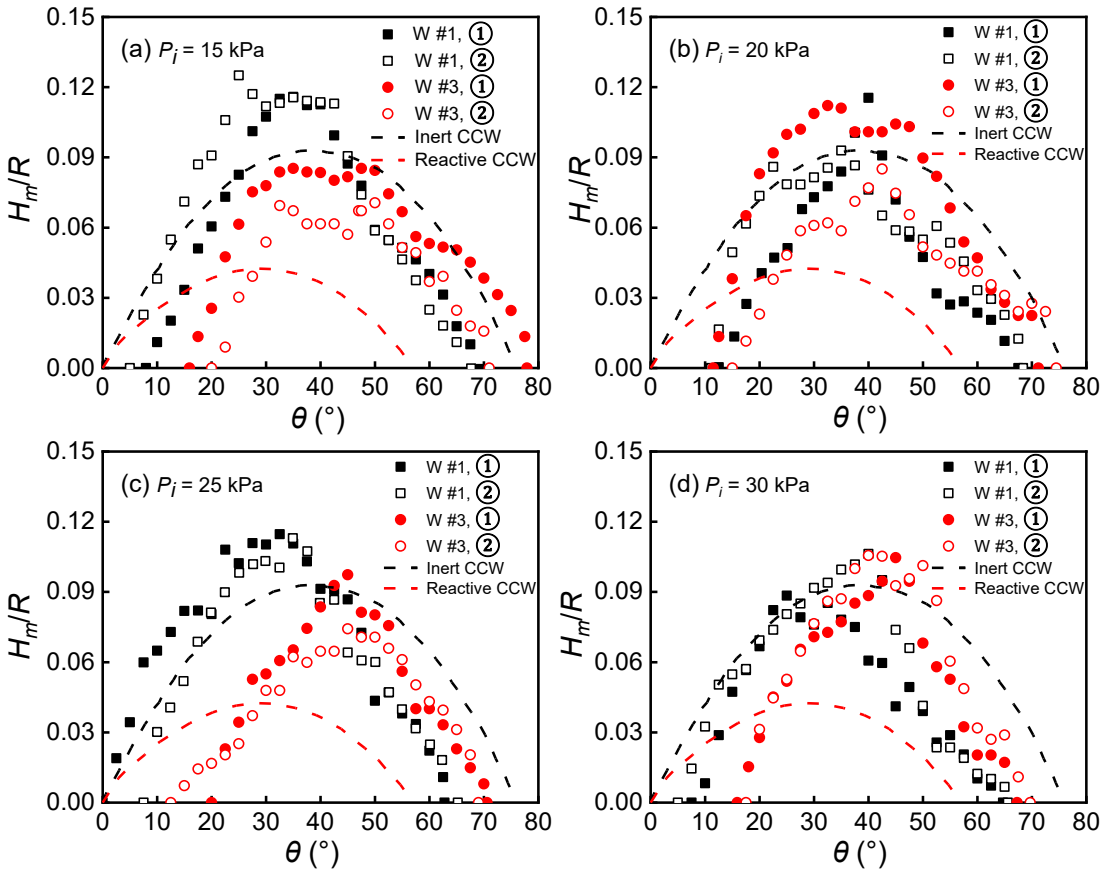


Fig. 6. The scaled Mach stem height H_m/R as a function of the angle θ over W#1 and W#3 in a stoichiometric $2H_2$–O_2–2Ar mixture.

The reflection process over a coupled wedge can be qualitatively interpreted using the double-plane-wedge framework proposed by Ben-Dor et al. [20], as illustrated in Fig. 7. A coupled wedge is defined as a concave double-wedge if $\Delta\theta_w > 0$ and a convex double-wedge if $\Delta\theta_w < 0$, where $\Delta\theta_w = \theta_{2w} - \theta_{1w}$, and θ_{1w} and θ_{2w} are the inclination angles of the front and rear wedges, respectively. The possible reflection configurations over the downstream wedge depend on θ₁w, θ₂w, and θcri, where θcri denotes the critical wedge angle for the MR→RR transition in detonation reflection. The lines $\theta_{1w} = \theta_{cri}$, $\theta_{2w} = \theta_{cri}$, $\Delta\theta_w = 0$, and $\Delta\theta_w = \theta_{cri}$ divide the (θ_{1w}, θ_{2w})-plane into seven typical regions. The regions above and below the diagonal $\Delta\theta_w = 0$ correspond to concave and convex double wedges, respectively.

The double-wedge framework in Fig. 7 provides a qualitative analogy for detonation reflection over the convex–concave surface. It is experimentally observed that the Mach stem (MS_1) has an included angle, θ^*_{1w}, of around 10° relative to OO', as it travels to the connection point O. Starting from point O, MS_1, as an incident wave, propagates along the concave surface of W#3 with its slope, θ_{2w}, gradually increasing from 0° to 90°. Indeed, the reflection of detonation waves over W#3 can be simplified as reflection over a plane wedge with $\theta_{1w} = 10°$, then over a second plane wedge with θ_{2w} ranging from 0° to 90°, corresponding to $OABQ$ in Fig. 7c. As θ_{2w} varies from 0° to θ^*_{1w} (~10°), $\Delta\theta_w < 0$; therefore, the process $O \rightarrow A$ for MS_1 is

analogous to that on a convex double-plane wedge (Fig. 7b). For a normally incident detonation wave propagating along a concave wedge, Mach reflection generally begins at the wedge tip, corresponding to a local wedge angle of approximately 0°. For MS_1, which enters the concave section at an inclination of θ^*_{1w}, secondary Mach reflection begins beyond A at a local wall angle approximately 10° larger than in the single-concave configuration. This angular shift is comparable to θ^*_{1w} (see arrow in Fig. 8). The process $A \rightarrow B$ is characterized by $\Delta\theta_w > 0$, during which the second Mach reflection occurs. As the detonation wave continues to propagate downstream and reaches point B, the condition $\theta_{2w} > \theta^*_{1w} + \theta_{cri}$ is observed. This phenomenon indicates the transition from MR to RR process.

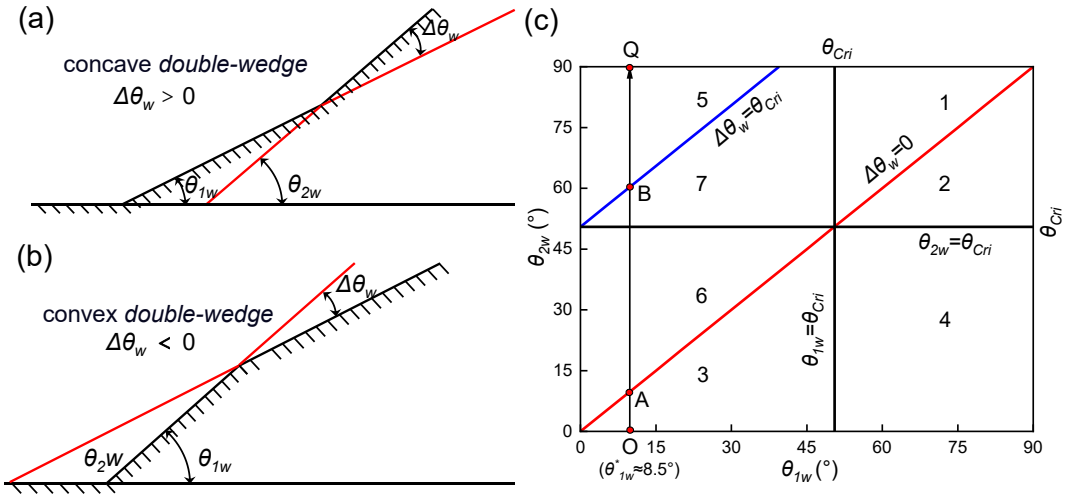


Fig. 7. (a) Schematic drawing of a concave double-wedge, (b) schematic drawing of a convex double-wedge, (c) classification of different reflection zone types in a double-wedge structure.

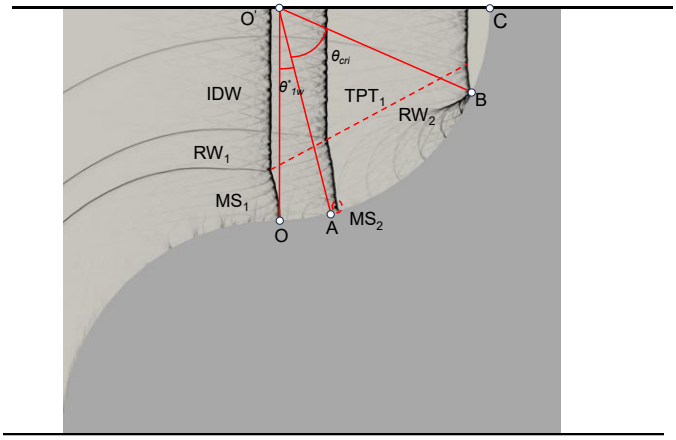


Fig. 8. Composite schlieren images showing the reflection process of a cellular detonation wave over W#3.

3.3 Numerical simulation of Mach reflection over convex-concave coupled wedges

To clarify the evolution of Mach reflection over the coupled wedges, numerical simulations were performed and compared with the experimental observations, as shown in Fig. 9. The simulations, which accurately reproduced the principal features of the experimentally observed reflection process, were implemented on the OpenFOAM-6 platform [21] utilizing the open-source solver detonationFoam developed by Sun et al. [22]. The specific details of the

numerical simulation are provided in the Appendix. At the early stage of Mach reflection over the convex surface, the numerical and experimental TPT_1 matches very well for the different wedges (Fig. 10); however, these two deviate as the Mach stem approaches the conjunction point of the wedges ($\theta = 0°$). This deviation increases as the convex wedge radii increase. Also, the increase of the convex radii directly leads to the increase of Mach stem height of TPT_1, as seen in Fig. 10. Interestingly, although there is large difference in TPT_1 at different R_1, TPT_2 is essentially the same. Specifically, TPT_2 starts roughly at $\theta = 10°$ and ends at $\theta = 70°$ over different wedges, which has a similar trend with an identical maximum height of approximately 3 mm. This indicates that the geometrical size of the forward convex wedge does not affect the second Mach reflection over the rear concave wedge. A careful examination of the numerical results reveals that the Mach stem entering the concave surface possesses an identical arc shape and a similar included angle (around 8.5°), as seen in Fig. 9a, 9b and 9c. Since the dominant factor governing Mach reflection is the angle between the incident wave and the reflecting surface, the behavior of the second Mach reflection is very similar regardless of the radius of the forward wedge.

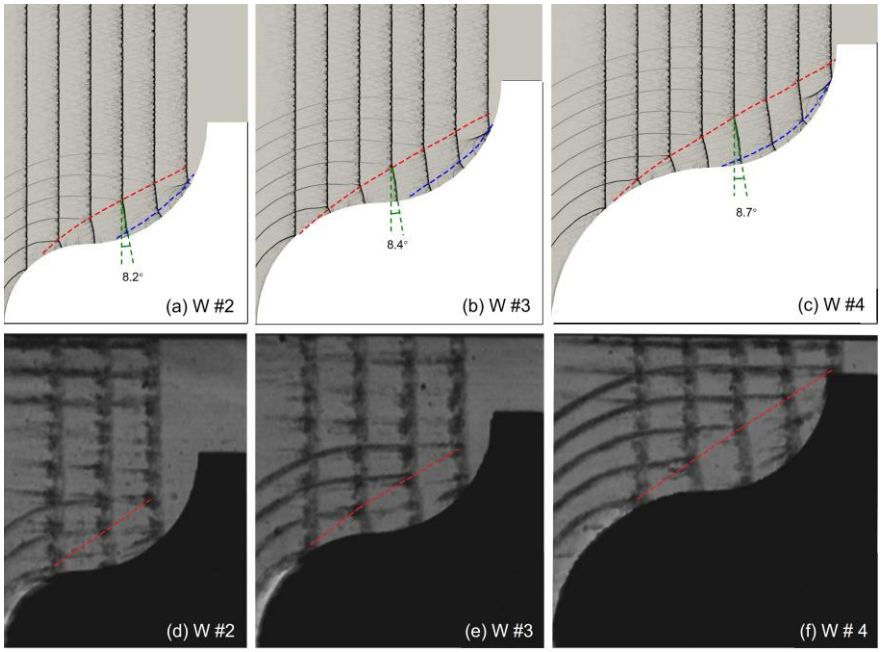


Fig. 9. Numerical (upper) and experimental (lower) composite schlieren images showing the reflection process of a cellular detonation wave over the wedges in a stoichiometric $2H_2$–O_2–2Ar mixture at P_i = 20 kPa.

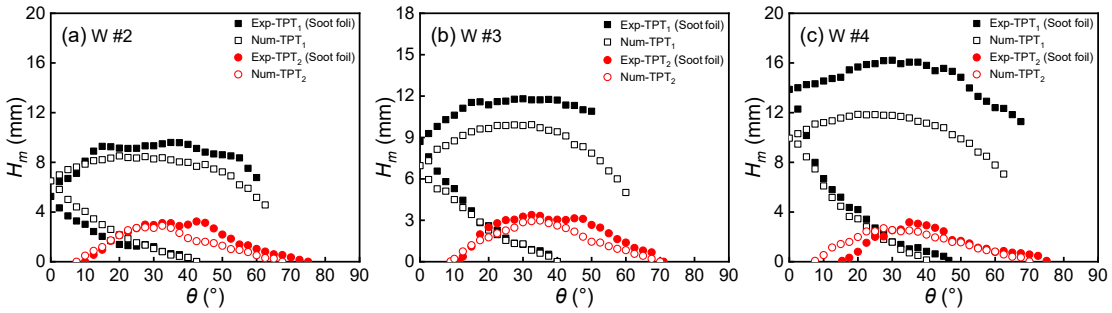


Fig. 10. Experimental and numerical triple-point trajectories over the wedges in a stoichiometric $2H_2$–

O_2–2Ar mixture at P_i = 20 kPa.

3.4 The critical wedge angle of Mach reflection

For the reflection of an incident detonation wave off a convex–concave coupled wedge, the critical wedge angles of the RR→MR transition over the convex surface (θ_1) and MR→RR transition over the concave surface (θ_2) are the key parameters that are analyzed in this section. It can be observed that θ_1 shows considerable scatter under all test conditions (Fig. 11a); nevertheless, the data are still bounded by the predictions of inert and reactive two-shock theory . The scatter slightly decreases as R/λ increases, as seen in Fig. 11b. This suggests that the RR→MR transition over the convex surface is a local behavior that is closely associated with the inherent instability of the cellular detonation. Although the data are highly dispersed, the average value is approximately 41°, which is in close agreement with the experimental results reported by Li et al. [18].

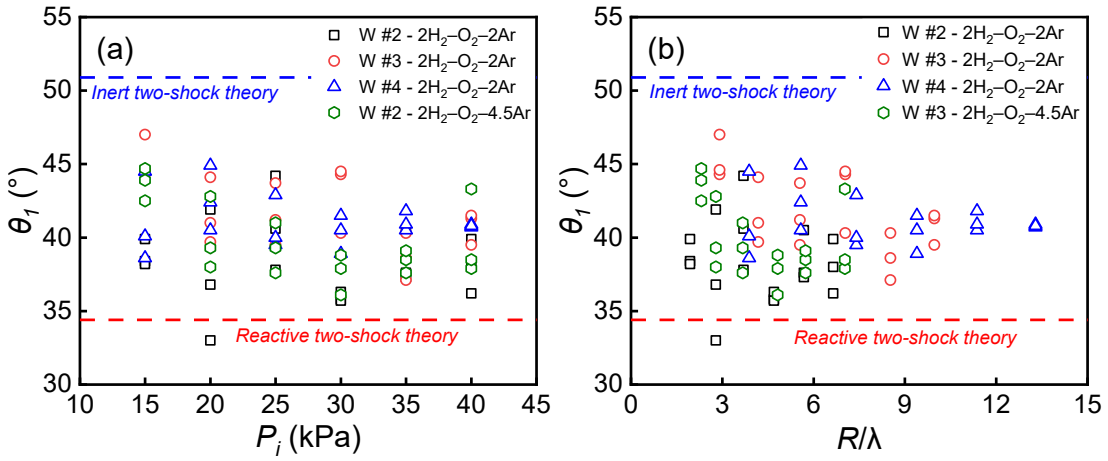


Fig. 11. The critical angle of RR→MR over the convex wedge θ_1 as a function of initial pressure P_i (a), and R/λ (b).

It is established that Mach reflection over the front wedge influences the onset angle of secondary Mach reflection over the rear wedge, thereby significantly affecting its termination angle (the MR→RR critical wedge angle, θ_2). Fig. 12 shows θ_2 as a function of P_i for different coupled wedges, and θ_2 for the single concave wedge (W#1) is also shown for reference. Notably, θ_2 obtained from the coupled wedges (W#2, W#3 and W#4) are larger than those from W#1, as seen in Fig. 12a and 12b. This is mainly associated with the incident wave that enters the concave surface. Recall that the incident wave over the concave surface of W#2, W#3, and W#4 is the Mach stem at an angle (see Fig. 9). The Mach stem requires a certain duration to respond to the influence of the angle; therefore, the Mach reflection process over the concave surfaces of W#2, W#3, and W#4 is delayed, yielding a larger θ_2. It can be clearly observed that, regardless of the wedge geometry and mixture composition, θ_2 exhibits the same decreasing trend as P_i (R/λ) increases, as shown in Fig. 12. This suggests that the MR→RR transition occurs earlier as the incident wave is stronger.

According to the "corner signal" theory [11], a Mach reflection can form only if a physical length scale signal generated from near the wedge tip communicates with the triple point, otherwise a regular reflection is formed. Because θ_2 at the MR→RR transition marks the limit beyond which Mach reflection cannot occur, this point also represents the limiting position at which the corner signal can communicate with the triple point. The corner signal velocity

propagates at a velocity of $u_s = u + a$, where u is the flow velocity and a is the local speed of sound. Obviously, u_s increases with P_i; therefore, at higher P_i, the corner signal reaches the triple point sooner, causing the MR→RR transition to occur earlier. This same is true for the more highly argon-diluted mixture in Fig. 12b, where θ_2 for $2H_2$–O_2–4.5Ar is larger than that for $2H_2$–O_2–2Ar.

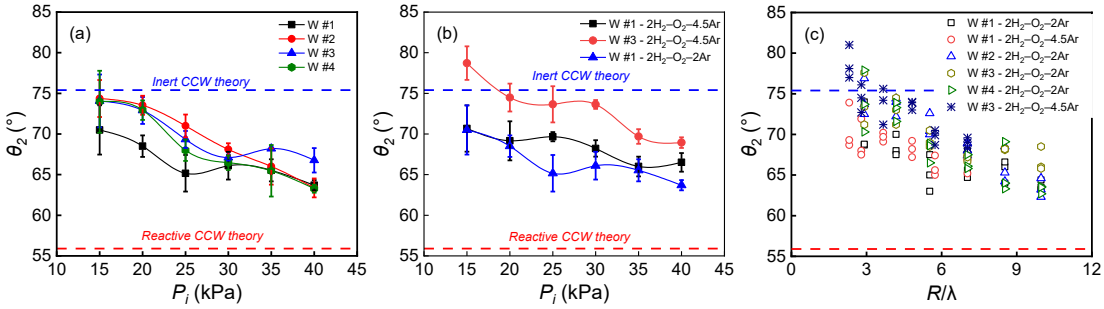


Fig. 12. The critical angle of MR→RR over the concave surface θ_2 in stoichiometric mixture of $2H_2$–O_2–2Ar (a), $2H_2$–O_2–4.5Ar (b), and θ_2 as a function of R/λ (c).

4 Conclusions

Mach reflections of cellular detonations over coupled convex–concave cylindrical surface were studied using schlieren imaging and soot foil technology, complemented by 2D numerical simulations. Notably, the convex surface gives rise to the first Mach reflection, in which the Mach stem acts as the incident wave that produce the second Mach reflection on the rear concave surface. The sequences of Mach reflection over the concave surface are almost identical for the coupled wedges and the single concave wedge. However, the difference is that both the onset and termination of the Mach reflection over the concave surface of the coupled wedges are delayed compared with those on the single concave wedge. The numerical simulations revealed that the first Mach stem becomes curved as it enters the rear concave surface. Furthermore, the configuration of the incident wave is critically important to the subsequent behavior of the Mach reflection. The parametric studies showed that the critical angle for the occurrence of Mach reflection exhibits large scatter, with an average value of 41°, and that the scatter decreases slightly with increasing initial pressure. This indicates that the geometric size of the forward convex surface does not affect the location of the first Mach reflection. The critical angle for the termination of the second Mach reflection on the concave surface shows a clear decreasing trend with increasing initial pressure.

Research funding

This work is supported by the National Natural Science Foundation of China (Grant No.12572412) and the National Key Laboratory of Shock Wave and Detonation Physics Fund (Grant No. JCKYS2026212102).

References

1. Mach, E.: Über den Verlauf von Funkenwellen in der Ebene und im Raume. Sitzungsbr. Akad. Wiss. Wien. 78, 819–838 (1878).
2. Ben-Dor, G.: Shock Wave Reflection Phenomena, 2nd edn. Springer, New York (2007).
3. von Neumann, J.: Oblique reflection of shocks. Explos. Res. Rep. 12, Navy Department, Bureau of Ordnance, Washington, DC, USA (1943)
4. von Neumann, J.: Refraction, intersection and reflection of shock waves. NAVORD Rep. 203-45, Navy Department, Bureau of Ordnance, Washington, DC, USA (1943)
5. Chester, W.: CXLV. The quasi-cylindrical shock tube. Philos. Mag. 45, 1293–1301 (1954). https://doi.org/10.1080/14786441208561138
6. Chisnell, R.F.: The motion of a shock wave in a channel, with applications to cylindrical and spherical shock waves. J. Fluid Mech. **2**, 286–298 (1957). https://doi.org/10.1017/S0022112057000130.
7. Whitham, G.B.: A new approach to problems of shock dynamics. Part 1. Two-dimensional problems. J. Fluid Mech. **2**, 145–171 (1957). https://doi.org/10.1017/S002211205700004X
8. Skews, B., Blitterswijk, A.: Shock wave reflection off coupled surfaces. Shock Waves **21**, 491–498 (2011). https://doi.org/10.1007/s00193-011-0334-y.
9. Geva, M., Ram, O., Sadot, O.: The non-stationary hysteresis phenomenon in shock wave reflections. J. Fluid Mech. **732**, R1 (2013). https://doi.org/10.1017/jfm.2013.423
10. Hornung, H.G., Smith, G.H.: The influence of relaxation on shock detachment. J. Fluid Mech. **93**, 225–239 (1979). https://doi.org/10.1017/S0022112079001865
11. Hornung, H.G., Oertel, H., Sandeman, R.J.: Transition to Mach reflexion of shock waves in steady and pseudosteady flow with and without relaxation. J. Fluid Mech. **90**, 541–560 (1979). https://doi.org/10.1017/S002211207900238X.
12. Shepherd, J., Schultz, E., Akbar, R.: Detonation diffraction. In: 22nd International Symposium on Shock Waves, pp. 18–23. Imperial College, UK (1999)
13. Fortin, Y., Liu, J., Lee, J.H.S.: Mach reflection of cellular detonations. Combust. Flame **162**, 819–824 (2015). https://doi.org/10.1016/j.combustflame.2014.09.003
14. Li, J., Lee, J.H.S.: Numerical simulation of Mach reflection of cellular detonations. Shock Waves **26**, 673–682 (2016). https://doi.org/10.1007/s00193-016-0668-6
15. Li, J., Ren, H., Wang, X., Ning, J.: Length scale effect on Mach reflection of cellular detonations. Combust. Flame **189**, 378–392 (2018). https://doi.org/10.1016/j.combustflame.2017.11.002
16. Yuan, X., Zhou, J., Mi, X., Ng, H.D.: Numerical study of cellular detonation wave reflection over a cylindrical concave wedge. Combust. Flame **202**, 179–194 (2019). https://doi.org/10.1016/j.combustflame.2019.01.018
17. Jiao, Y., Ma, H.H., Wang, L.Q.: Quasi-detonation reflection over cylindrical wedges. Phys. Fluids **37**, 084133 (2025). https://doi.org/10.1063/5.0277374
18. Li, J., Ning, J.: Experimental and numerical studies on detonation reflections over cylindrical convex surfaces. Combust. Flame **198**, 130–145 (2018). https://doi.org/10.1016/j.combustflame.2018.07.017
19. Li, Q., Zhou, G., Pan, C., Xu, Z., Wang, C.: Mach reflections of a cellular detonation on a split wedge. Combust. Flame **273**, 113962 (2025). https://doi.org/10.1016/j.combustflame.2024.113962

20. Ben-Dor, G., Dewey, J.M., Takayama, K.: The reflection of a plane shock wave over a double wedge. J. Fluid Mech. **176**, 483–520 (1987). https://doi.org/10.1017/S0022112087000776
21. Jasak, H.: OpenFOAM: Open source CFD in research and industry. Int. J. Nav. Archit. Ocean Eng. **1**, 89–94 (2009). https://doi.org/10.3744/jnaoe.2009.1.2.089
22. Sun, J., Wang, Y., Tian, B., Chen, Z.: detonationFoam: An open-source solver for simulation of gaseous detonation based on OpenFOAM. Comput. Phys. Commun. **292**, 108859 (2023). https://doi.org/10.1016/j.cpc.2023.108859

Appendix

The configuration of the computational domain is illustrated in Fig. 13. Initially, the computational domain is filled with a stationary $2H_2 + O_2 + 2Ar$ mixture to generate stable detonation waves with regular cellular structures. The initial conditions are set as an initial temperature T_0 = 300 K and an initial pressure P_0 = 20 kPa. The numerical simulation framework employs a coupled rectangular and curved computational domain. The rectangular part has a length (Bottom) of 200 mm and a width of 80 mm. The boundary conditions are configured as follows: both the left and right sides are adiabatic non-reflective boundaries, while the lateral walls and the wedge-shaped body are adiabatic slip boundaries. The detonation wave is initiated by five equally spaced high-energy regions (with dimensions of 8 × 8 mm) set up at the closed left end. The initial parameters for each high-energy region are as follows: pressure $P_i = 20P_0$ and temperature $T_i = 10T_0$.

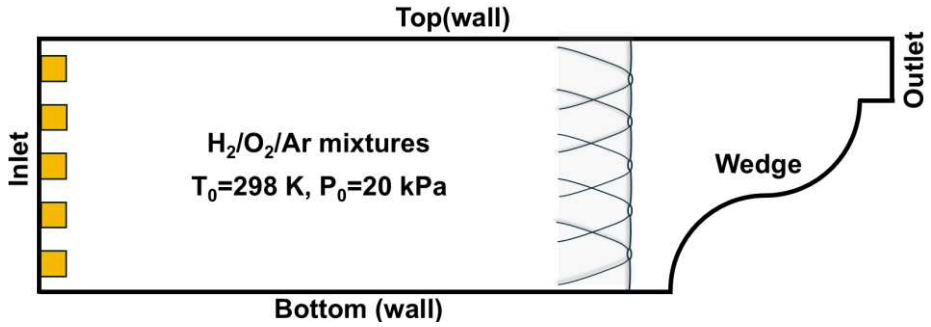


Fig. A1. Schematic of the simulation domain and settings

Since viscosity and thermal diffusion are neglected, the aforementioned flow problem was solved using the two-dimensional reactive Euler equations, with the corresponding expressions as follows:

$$\frac{\partial \boldsymbol{U}}{\partial t} + \frac{\partial \boldsymbol{E}}{\partial x} + \frac{\partial \boldsymbol{F}}{\partial y} = \boldsymbol{S} \tag{1}$$

$$\boldsymbol{U} = \begin{bmatrix} \rho \\ \rho u \\ \rho v \\ \rho e \\ \rho Y_i \end{bmatrix} \quad \boldsymbol{E} = \begin{bmatrix} \rho u \\ \rho u^2 + p \\ \rho uv \\ (\rho e + p)u \\ \rho u Y_i \end{bmatrix} \quad \boldsymbol{F} = \begin{bmatrix} \rho v \\ \rho uv \\ \rho v^2 + p \\ (\rho e + p)v \\ \rho v Y_i \end{bmatrix} \quad \boldsymbol{S} = \begin{bmatrix} 0 \\ 0 \\ 0 \\ 0 \\ \omega_i \end{bmatrix} \tag{2}$$

In the equations above, ρ is density, u and v represent the velocity components in the x-direction and y-direction within the Cartesian coordinate system, respectively, p is pressure, E is the total energy, Y_i is the mass fraction of species, S is the source term in the energy equation, and w_i is the production/consumption rate of species. The total energy E can be calculated using the following formula:

$$\begin{cases} E = h - \dfrac{p}{\rho} + \dfrac{1}{2}\left(u^2 + v^2\right) \\ h = \sum_{i=1}^{N_s} Y_i h_i \\ h_i(T) = h_{\mathrm{ref}}^0 + \int_{T_{\mathrm{ref}}}^{T} C_{p,i} dT \\ C_{p,i}(T) = \dfrac{R_u}{W_i}\left(a_{1,i} + a_{2,i}T + a_{3,i}T^2 + a_{4,i}T^3 + a_{5,i}T^4\right) \\ p = \sum p_i = \sum \rho Y_i R_i T = \sum_{i=1}^{N_s} \rho Y_i \dfrac{R_u}{W_i} T \end{cases} \tag{3}$$

Where, h is the total enthalpy, h_i is the specific enthalpy of component i, W_i is the molecular mass of component i, and T is the gas temperature. The universal gas constant R_u is equal to 8.31451 J/(mol·K). Assuming that all component gases behave as ideal gases, they satisfy the ideal gas law. By utilizing the aforementioned equations, the temperature T and pressure p can be determined.

The simulations were implemented on the OpenFOAM-6 platform, utilizing the open-source solver detonationFoam developed by Sun et al. This solver is specifically tailored for the precise and efficient simulation of detonation processes. A multitude of researchers have utilized it to investigate detonation problems and have validated its accuracy in simulating compressible multi-component reactive flows. The numerical methods adopted are as follows: To address the stiffness issue inherent in chemical reactions, this solver employs the operator splitting fractional-step procedure to solve the convective terms. In terms of spatial discretization, face-centered values are reconstructed from cell-centered data using a second-order MUSCL scheme, while convective fluxes are computed utilizing a modified approximate Riemann solver, HLLC-P. For the diffusion terms, a second-order central difference scheme is adopted. Time integration is performed using a first-order implicit Euler scheme, with automatic time-step adjustment implemented to ensure that the Courant number remains below 0.2. The stiff ordinary differential equation solver, Seulex, is used to handle the chemical reactions. In all simulations, a simplified chemical reaction mechanism for hydrogen-oxygen mixtures is adopted, which comprises 10 species and 27 elementary reactions and has been proven effective for detonation simulations. To capture the fine-scale structures of detonation, high-resolution grids are required in the shock front region, whereas coarser grids are employed in other regions with relatively smooth flow behaviors to reduce computational costs. Consequently, adaptive mesh refinement (AMR) technology is implemented during the simulations to dynamically optimize grid distribution, combined with a dynamic load balancing algorithm to enhance computational efficiency.